Elastic Differential Cross Sections for $\pi^{\pm}+p$ Scattering from 2.3–6.0 BeV/c*

C. T. COFFIN, N. DIKMEN, L. ETTLINGER,† D. MEYER, A. SAULYS,‡ K. TERWILLIGER, AND D. WILLIAMS§
University of Michigan, Ann Arbor, Michigan

(Received 20 February 1967)

Elastic differential cross sections were measured at 6 energies between 2.3 and 6 BeV/c for $\pi^+ + p$ and $\pi^- + p$. The behavior of the secondary peak as a function of energy and charge is shown. Evidence for considerable resonance structure is seen in the angular distributions.

INTRODUCTION

IN two previous papers[1,2] we have presented partial results of an experiment to measure the differential cross section in $\pi^{\pm}+p$ elastic scattering. We would like to present here the complete results at all momenta. The experiment was run at the Argonne ZGS accelerator, using a π-meson beam from an internal target. The π^- momenta studied were 2.5, 3.0, 3.5, 4.0, 5.0, and 6.0 BeV/c. The π^+ momenta were 2.3, 2.5, 2.7, 3.0, 3.5, 3.7, and 4.0 BeV/c. Because of bending by the magnetic field of the accelerator, it was not possible to take data above 4.0 BeV/c for the π^+ mesons.

The purpose of the experiment was to do a systematic survey of the elastic scattering process. Specifically, we wanted to investigate the slope of the diffraction peak, the energy and charge dependence of the secondary peak appearing at $-t\sim 1$ BeV^2, the presence or absence of a peak at scattering angles near 180°, and structure in the intermediate-angle region.

A total of 750 000 pictures were taken, containing 150 000 elastic scattering events.

APPARATUS

The experiment was carried out with an array of spark chambers and counters shown in Fig. 1. The spark chambers subtended a relatively small azimuthal angle giving an acceptance of approximately 1/20 for elastic scattering events. The twelve spark chambers were placed to give approximately equal azimuthal acceptance at all polar angles. They were arranged so that all tracks passed through at least two chambers 12 in. apart at angles of 45° or less. The liquid-hydrogen target was 12 in. long by 1½ in. in diameter.

Pictures were taken of the spark chamber array through a 4-ft diam Plexiglas field lens with a 30-ft focal length. Fiducial marks for the pictures consisted of electroluminescent panels.[3] A camera developed at Michigan[4] capable of advancing the film in 25 msec allowed a picture taking rate of up to 7 frames per pulse.

The beam used in the experiment left the ZGS accelerator at an angle of 17°. Because of the bending in the accelerator magnetic field, the production angle of the particles accepted by the beam was 0° for π^- and 17° for π^+ mesons. Because of the large production angle, there was a considerable proton contamination in the π^+ beam. The beam consisted of two sections of bending and focusing and gave a spot size at the hydrogen target of approximately ⅜ in. The divergence was ± 3 mrad at the target.

The protons in the beam were rejected by two methods. Both a threshold Čerenkov counter and a time-of-flight system with counters at the first and second beam foci were used. The electron contamination in the beam was measured by running the Čerenkov counter at low-gas pressure below π- and μ-meson threshold and was found to be 1% or less. The μ contamination was measured by absorbing out the π mesons. It varied from 3–5% with energy.

In addition to the beam counters, an anticoincidence of counter 4 plus counts in one left-side and one right-side counter were required to trigger the spark chambers. The azimuthal angle was defined by these side counters. The efficiency of these side counters was tested in the beam at several points along their length and found to be greater than 99%.

ANALYSIS OF PICTURES

The large number of pictures and events involved made the use of some device to automatically scan and measure pictures mandatory. A flying spot scanner attached to a digital computer was developed to carry out this analysis.[5] Approximately 90% of the events were found and analyzed automatically.

The pictures were then all scanned by hand to pick up events which the automatic scanner had missed. A sample was then rescanned to check scanner efficiency. Finally all events in the angular region where the cross section was low enough to make background a problem were measured by hand since the accuracy thus obtain-

* Supported by the U. S. Atomic Energy Commission.
† Present address: Johns Hopkins University, Baltimore, Maryland.
‡ Present address: DESY, Hamburg, Germany.
§ Present address: General Dynamics Corporation, Groton, Connecticut.
[1] C. T. Coffin *et al.*, Phys. Rev. Letters **15**, 838 (1965).
[2] C. T. Coffin *et al.*, Phys. Rev. Letters **17**, 458 (1966).
[3] A. Saulys and E. Meanley, Rev. Sci. Instr. **36**, 1053 (1965).
[4] Developed by O. Haas.
[5] A. Saulys, D. Meyer, and R. Allen, Nucl. Instr. Methods **39**, 335 (1966).

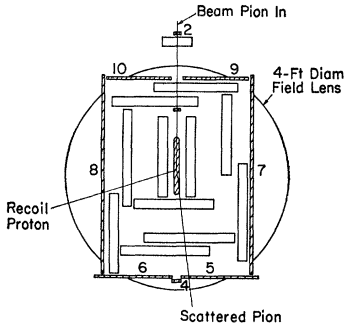

FIG. 1. Plan view of apparatus.

able was approximately twice that available on the automatic scanner.

Identification of events was based on two criteria, coplanarity and kinematically predicted angles. The measurement errors allowed these angles to be determined to about 3 mrad. There were several checks on this accuracy: the origin fit of the incoming track with the two outgoing tracks, and the coplanarity and kinematics fit to elastic scattering in angular regions where background was negligible. It was found that at the large angles where the cross section was small the background due to inelastic events was less than 0.5 μb/sr. At these angles a scatter plot was made of distance from the kinematics curve versus deviation from coplanarity. Except at the higher π^- energies in certain angular regions where only upper limits are reported on the cross section, it was quite easy to separate the events from background.

No attempt was made to look at very small forward or backward scattering angles although there were events in these regions. In the forward direction ($\cos\theta > 0.98$), the solid angle acceptance became too uncertain to allow reliable results. In addition, many of the protons had such a short range or scattered so much that measurements were unreliable. In the backward

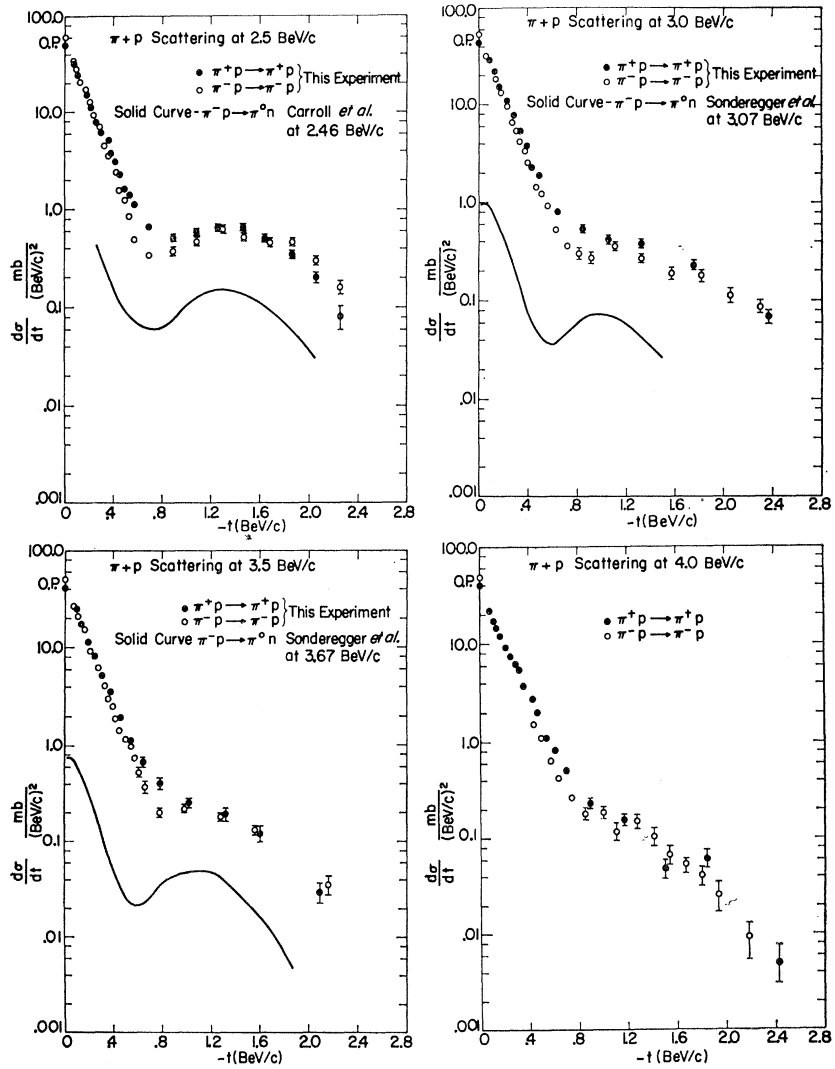

FIG. 2. Comparison of $\pi^+ + p$, $\pi^- + p$ elastic scattering and $\pi^- + p$ charge-exchange scattering in the forward and secondary peak regions at 2.5, 3.0, 3.5, and 4.0 BeV/c. The charge-exchange curves are from Refs. 9 and 10. O.P. is the optical point determined from the total cross section.

TABLE I. πp elastic scattering.

$-t$ (BeV/c)^2	$d\sigma/dt$ mb/(BeV/c)^2	Error mb/(BeV/c)^2
	2.5 BeV/c $\pi^- p$	
0.069	34.46	0.90
0.088	28.42	0.83
0.108	24.87	0.74
0.128	21.67	0.70
0.147	18.60	0.64
0.167	16.27	0.58
0.187	14.42	0.58
0.206	12.95	0.54
0.226	10.61	0.48
0.246	9.56	0.45
0.265	8.02	0.42
0.285	7.10	0.39
0.305	5.75	0.35
0.325	4.54	0.31
0.344	3.64	0.27
0.364	3.58	0.27
0.383	2.59	0.23
0.413	2.41	0.16
0.452	1.66	0.13
0.491	1.24	0.12
0.531	0.825	0.089
0.570	0.480	0.074
0.688	0.329	0.035
0.884	0.374	0.038
1.08	0.473	0.048
1.29	0.620	0.054
1.47	0.521	0.048
1.67	0.467	0.045
1.87	0.470	0.048
2.06	0.302	0.035
2.26	0.160	0.024
2.46	0.053	0.014
2.65	0.029	0.012
2.85	0.014	0.005
3.05	0.025	0.008
3.24	0.031	0.008
3.44	0.041	0.011
3.64	0.138	0.018
3.77	0.162	0.029
3.86	0.106	0.019
	3.0 BeV/c $\pi^- p$	
0.085	27.5	0.7
0.109	22.1	0.6
0.133	18.7	0.6
0.157	16.0	0.5
0.182	13.6	0.5
0.206	11.9	0.5
0.230	9.9	0.4
0.254	7.05	0.36
0.278	6.71	0.36
0.303	5.50	0.31
0.327	4.29	0.28
0.311	3.94	0.25
0.375	3.40	0.25
0.400	2.58	0.22
0.425	2.13	0.20
0.450	2.03	0.19
0.474	1.46	0.16
0.110	1.26	0.11
0.559	0.93	0.09
0.630	0.53	0.05
0.727	0.366	0.04
0.824	0.305	0.038
0.921	0.274	0.037
1.09	0.362	0.036
1.33	0.272	0.028
1.58	0.191	0.026
1.82	0.181	0.023
2.06	0.114	0.018
2.30	0.088	0.013
2.55	0.031	0.008
2.79	0.010	0.005
3.04	0.005	0.003
3.28	0.034	0.008
3.52	0.039	0.008
3.76	0.023	0.008
4.01	0.029	0.008
4.24	0.034	0.008
4.48	0.021	0.008
4.72	0.026	0.008
	3.5 BeV/c $\pi^- p$	
0.072	27.19	0.66
0.101	21.77	0.58
0.130	18.58	0.53
0.159	15.59	0.48
0.187	11.58	0.41
0.216	9.21	0.37
0.245	8.05	0.34
0.274	6.37	0.30
0.303	5.18	0.27
0.332	4.27	0.25
0.361	3.13	0.21
0.390	2.61	0.19
0.415	1.95	0.17
0.447	1.48	0.15
0.476	1.59	0.15
0.505	1.18	0.13
0.534	0.996	0.120
0.563	0.750	0.106
0.606	0.539	0.063
0.664	0.377	0.055
0.779	0.204	0.022
1.01	0.225	0.015
1.30	0.182	0.018
1.59	0.132	0.015
1.87	0.087	0.014
2.16	0.037	0.008
2.45	0.0053	0.0036
2.74	0.002	0.002
3.03	0.002	0.002
3.32	0.0056	0.0031
3.61	0.0092	0.0039
3.90	0.016	0.005
4.18	0.0047	0.0028
4.47	<0.001	...
4.76	0.002	0.002
5.05	0.002	0.002
5.34	0.0044	0.0026
5.61	0.0074	0.0035
	4.0 BeV/c $\pi^- p$	
0.084	23.47	0.59
0.117	18.72	0.56
0.151	14.52	0.48
0.184	11.27	0.43
0.218	8.54	0.38
0.251	6.73	0.33
0.285	5.23	0.29
0.318	4.18	0.26
0.368	3.13	0.16
0.435	1.74	0.12
0.503	1.20	0.10
0.570	0.71	0.08
0.637	0.47	0.06
0.737	0.277	0.034
0.871	0.193	0.027
1.00	0.195	0.027
1.14	0.124	0.024
1.27	0.158	0.025
1.41	0.110	0.024
1.54	0.071	0.016
1.67	0.057	0.012
1.81	0.040	0.009
1.94	0.027	0.009
2.18	0.0098	0.004
2.51	0.0059	0.004
2.68–6.03	<0.002	...
6.20	0.0020	0.0014
6.51	0.0110	0.004
	5.0 BeV/c $\pi^- p$	
0.107	18.450	0.608
0.150	14.403	0.518
0.193	10.316	0.443
0.235	7.402	0.377
0.278	5.587	0.323
0.321	3.934	0.270
0.369	3.121	0.242
0.406	2.205	0.204
0.471	1.361	0.113
0.556	0.798	0.087
0.649	0.365	0.059
0.727	0.318	0.054
0.813	0.199	0.043
1.070	0.122	0.015
1.498	0.063	0.011
1.925	0.018	0.006
2.353	0.012	0.005
4.706	<0.002	
7.487	0.004	0.002
8.322	0.023	0.008
	6.0 BeV/c $\pi^- p$	
0.13	12.98	0.39
0.182	9.52	0.33
0.235	6.72	0.28
0.286	4.25	0.22
0.339	2.75	0.18
0.391	1.67	0.14
0.444	1.21	0.12
0.495	1.00	0.11
0.574	0.621	0.063
0.678	0.277	0.041
0.782	0.134	0.030
0.939	0.070	0.015
1.17	0.063	0.013
1.43	0.018	0.007
1.69	0.017	0.007
1.95	0.0070	0.0047
3.65–7.56	<0.001	...
10.12	0.0035	0.0024
	2.3 BeV/c $\pi^+ p$	
0.062	31.2	1.0
0.080	29.4	0.9
0.098	25.0	0.8
0.116	22.4	0.8
0.134	20.4	0.7
0.152	19.6	0.7
0.169	17.5	0.7
0.187	15.0	0.6
0.205	13.9	0.6
0.223	11.5	0.6
0.241	11.9	0.6
0.259	9.1	0.5
0.276	7.1	0.4

TABLE I (*continued*)

$-t$ (BeV/c)^2	$d\sigma/dt$ mb/(BeV/c)^2	Error mb/(BeV/c)^2
0.294	7.45	0.45
0.312	6.7	0.4
0.330	6.8	0.4
0.348	5.9	0.4
0.374	4.7	0.25
0.410	3.7	0.2
0.446	3.1	0.2
0.481	2.35	0.18
0.517	1.66	0.16
0.624	1.17	0.06
0.802	0.69	0.05
0.981	0.67	0.05
1.16	0.74	0.05
1.34	0.87	0.05
1.12	0.69	0.05
1.69	0.55	0.04
1.87	0.41	0.035
2.05	0.36	0.035
2.23	0.27	0.03
2.41	0.29	0.03
2.59	0.26	0.03
2.76	0.188	0.02
2.94	0.169	0.02
3.12	0.143	0.02
3.30	0.161	0.02
3.42	0.222	0.04
3.50	0.356	0.04
	2.5 BeV/c π^+p	
0.069	32.80	1.0
0.088	28.30	0.96
0.108	24.6	0.8
0.128	21.7	0.8
0.147	20.6	0.8
0.167	18.5	0.7
0.187	15.3	0.7
0.206	13.1	0.6
0.226	11.2	0.5
0.246	10.2	0.5
0.265	7.90	0.48
0.285	8.28	0.48
0.305	6.14	0.41
0.324	6.65	0.41
0.344	5.24	0.38
0.364	5.31	0.38
0.383	3.80	0.32
0.413	3.10	0.21
0.452	2.34	0.18
0.491	1.60	0.15
0.531	1.43	0.14
0.570	1.13	0.13
0.688	0.671	0.044
0.884	0.505	0.038
1.08	0.585	0.044
1.29	0.649	0.048
1.47	0.658	0.048
1.67	0.118	0.038
1.87	0.352	0.035
2.06	0.202	0.026
2.26	0.082	0.022
2.46	0.133	0.021
2.65	0.147	0.022
2.85	0.130	0.020
3.05	0.143	0.021
3.24	0.185	0.023
3.44	0.207	0.024
3.64	0.142	0.019
3.77	0.261	0.043
3.86	0.464	0.045

$-t$ (BeV/c)^2	$d\sigma/dt$ mb/(BeV/c)^2	Error mb/(BeV/c)^2
	2.7 BeV/c π^+p	
0.054	32.7	1.0
0.075	29.0	0.9
0.097	26.8	0.9
0.118	22.7	0.8
0.140	18.6	0.7
0.161	17.4	0.7
0.183	15.3	0.6
0.204	13.15	0.6
0.226	10.2	0.5
0.247	9.0	0.5
0.269	7.8	0.5
0.290	7.5	0.4
0.312	6.55	0.4
0.333	5.38	0.4
0.355	4.73	0.4
0.376	3.80	0.3
0.398	3.28	0.3
0.419	2.31	0.25
0.411	2.37	0.18
0.494	1.55	0.15
0.537	1.26	0.13
0.580	0.94	0.11
0.623	0.67	0.10
0.752	0.40	0.03
0.967	0.51	0.04
1.182	0.45	0.05
1.40	0.52	0.04
1.61	0.42	0.04
1.83	0.33	0.03
2.04	0.16	0.02
2.26	0.091	0.017
2.47	0.039	0.011
2.69	0.039	0.011
2.90	0.050	0.012
3.12	0.066	0.014
3.33	0.123	0.019
3.55	0.149	0.020
3.76	0.184	0.023
3.98	0.216	0.026
4.13	0.212	0.053
4.22	0.458	0.068
	3.0 BeV/c π^+p	
0.085	29.08	1.13
0.109	26.17	1.05
0.133	22.07	0.98
0.157	18.61	0.87
0.182	15.58	0.82
0.206	14.67	0.80
0.230	11.03	0.68
0.254	9.15	0.61
0.291	7.96	0.40
0.339	5.21	0.35
0.388	3.83	0.28
0.436	2.20	0.21
0.510	1.91	0.15
0.642	0.811	0.073
0.848	0.545	0.051
1.09	0.417	0.045
1.33	0.390	0.041
1.76	0.232	0.024
2.36	0.070	0.011
2.97	0.026	0.007
3.58	0.071	0.011
4.01	0.129	0.022
4.24	0.122	0.022

$-t$ (BeV/c)^2	$d\sigma/dt$ mb/(BeV/c)^2	Error mb/(BeV/c)^2
4.48	0.071	0.016
4.72	0.113	0.022
	3.5 BeV/c π^+p	
0.101	21.4	0.9
0.130	17.5	0.8
0.159	13.9	0.7
0.187	11.7	0.6
0.216	9.25	0.59
0.245	8.36	0.57
0.274	7.31	0.52
0.303	5.29	0.43
0.332	4.29	0.39
0.375	3.66	0.26
0.447	1.99	0.16
0.534	1.15	0.12
0.635	0.684	0.080
0.779	0.409	0.052
1.01	0.252	0.030
1.30	0.194	0.028
1.59	0.120	0.023
2.09	0.030	0.007
2.81	0.006	0.003
3.53	0.016	0.005
4.26	0.014	0.005
4.76	0.027	0.010
5.05	0.014	0.005
5.34	0.023	0.009
5.61	0.025	0.010
	3.7 BeV/c π^+p	
0.108	21.42	0.89
0.138	17.93	0.81
0.169	14.66	0.71
0.200	9.33	0.57
0.230	8.96	0.55
0.261	6.93	0.49
0.292	6.59	0.48
0.338	4.38	0.28
0.399	2.87	0.22
0.461	1.89	0.18
0.553	1.13	0.10
0.691	0.532	0.061
0.845	0.352	0.051
0.998	0.188	0.037
1.15	0.228	0.041
1.38	0.137	0.023
1.69	0.065	0.016
2.23	0.021	0.006
2.99	0.003	0.002
3.76	0.004	0.002
4.53	0.016	0.005
5.07	0.027	0.010
5.38	0.027	0.010
5.68	0.028	0.010
5.97	0.036	0.011
	4.0 BeV/c π^+p	
0.084	22.40	0.73
0.117	17.92	0.64
0.151	15.00	0.58
0.184	12.52	0.54
0.218	9.30	0.47
0.251	7.49	0.41
0.285	6.29	0.38
0.318	5.68	0.36
0.352	3.71	0.30
0.402	2.83	0.19

TABLE I (*continued*)

$-t$ (BeV/c)^2	$d\sigma/dt$ mb/(BeV/c)^2	Error mb/(BeV/c)^2	$-t$ (BeV/c)^2	$d\sigma/dt$ mb/(BeV/c)^2	Error mb/(BeV/c)^2	$-t$ (BeV/c)^2	$d\sigma/dt$ mb/(BeV/c)^2	Error mb/(BeV/c)^2
0.459	2.06	0.15	1.17	0.156	0.019	4.10	0.004	0.002
0.536	1.11	0.11	1.51	0.049	0.011	4.96	0.004	0.002
0.604	0.83	0.09	1.84	0.062	0.013	5.53	0.015	0.006
0.704	0.51	0.074	2.43	0.005	0.002	5.87	0.036	0.010
0.89	0.234	0.026	3.26	0.003	0.002	6.20	0.019	0.007
						6.52	0.028	0.009

direction ($\cos\theta < -0.985$), the target supports attenuated or scattered the backward-going π mesons so that again measurement was impossible.

The azimuthal solid angle acceptance was found for each event separately. This was done by performing a rotation of each event around the incoming track and determining the angular acceptance by the angle where one of the outgoing tracks intercepted the counter edges, the other outgoing track being within the counter. The original choice of geometry was such that the angular acceptance of an event rarely differed from the mean value by more than 10%.

A number of small corrections were needed to the angular distribution and several more to the over-all normalization of the data. Some of these have been mentioned previously.

(1) *Coulomb scattering and stopping.* These required correction only for the very low-energy protons and hence only in the very forward direction where the cross section was large. Since the background was negligible in this region, we could relax our requirements on coplanarity and kinematics sufficiently so that we accepted essentially all of these events. Because there were mirrors and other needed supports scattered among the spark chambers, some low-energy protons were stopped before reaching the outside set of spark chambers. This correction varied from energy to energy but was of the order of 10% for the smallest angle reported, and 3% for the next angular bin.

(2) *Interactions in the target.* Corrections had to be made for the probability of interaction of both the incoming and outgoing particles. Because of the dependence of cross section on energy, these varied slightly from bin to bin and energy to energy. They were typically about 5% and varied about 1% from angle to angle.

(3) *μ and electron contamination in the beam.* These required about a 5% correction.

(4) *Occlusion by target supports in backward direction.* This caused a cutoff beyond $\cos\theta^* = -0.98$.

(5) *Scanning inefficiency.* Because tracks at 45° to spark-chamber plates were more difficult to see than those perpendicular to the plates, there was an angular bias in both the automatic and human scanning. By carefully rescanning a fraction of the pictures, we were able to determine this scanning inefficiency. It was less than 1% on the diffraction peak, 15% at intermediate angles, and 10% in the far backward direction. In all cases it was less than the statistical errors.

(6) *Events in wrong angular interval.* Because of small measurement errors, an event could be placed in the wrong angular interval. This effect averages out except in the diffraction peak where the steep slope and small angular bins might cause a problem. Even here, however, the measurement accuracy was such as to make the effect negligible. A more serious problem was the angular interval in which the kinematics made it impossible to decide which outgoing particle was the proton and which the π. Because the measurement accuracy was high, the angular interval over which the trouble occurred only involved two bins around $\cos\theta^* = -0.1$ where the cross section typically was relatively constant. The choice of bins was made on a statistical basis weighted by the distance of the event from the kinematics curve with the two different choices.

(7) Corrections had to be made for unscannable pictures and where extra beam tracks made measurement impossible. The second of these is probably the biggest source of error in the absolute normalization. The correction was as large as 10% at some energies where there were many protons in the beam. The error on the correction is $\pm 3\%$.

RESULTS

The results of the experiment are shown in Table I. In addition to the errors shown on the individual points, a $\pm 5\%$ over-all normalization error should be included.

The discussion of the results may be naturally divided into four regions:

(1) the diffraction peak; (2) the secondary peak at $-t \sim 1.0$ (BeV/c)^2; (3) the intermediate region (At the lower energies the secondary peak extends back so far that this region practically doesn't exist.); (4) the far backward region.

In the diffraction-peak region there are several interesting conclusions. Out to $-t \sim 0.5$ (BeV/c)^2, the data are fit by an exponential. The slope for both $\pi^+ + p$ and $\pi^- + p$ scattering is constant with energy within experimental error. There is, however, a definite difference in slope between π^+ and π^-. Using $d\sigma/dt = Ae^{Bt}$ the π^+ slope is $B = 6.7 \pm 0.2$ and the π^- slope is 7.4 ± 0.2.

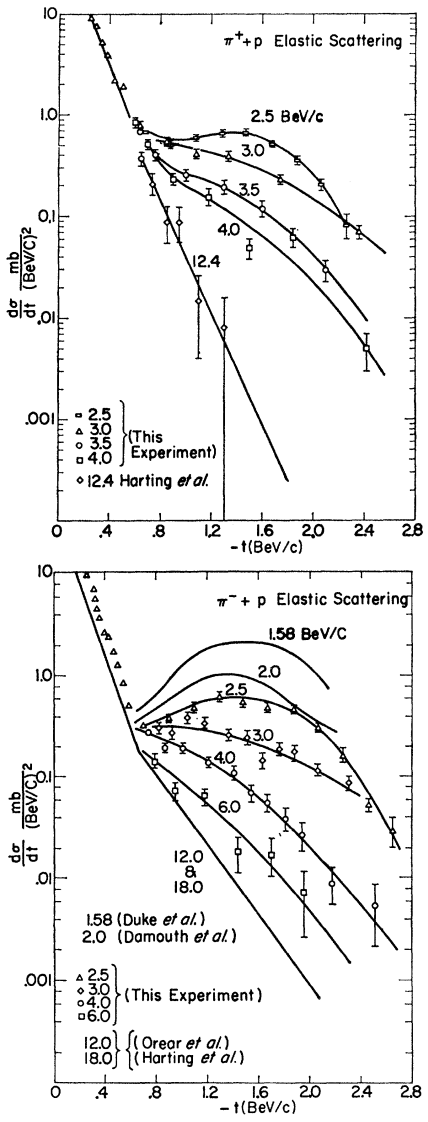

FIG. 3. Momentum dependence of the secondary peak in $\pi^+ + p$ and $\pi^- + p$ scattering. The low- and high-energy data are from Refs. 6, 7, and 8.

These are consistent with other results at higher and lower energies.[6–8]

Our data extrapolated to $t=0$ are consistent with the optical point determined by the total-cross-section data plus corrections for the real part of the forward-scattering amplitude determined by dispersion theory. The experiment is not ideal to determine the intersection at $t=0$, however, as the extrapolation is rather long.

In the secondary-peak region, both the energy dependence and charge dependence of the peak are striking effects. The $\pi^+ + p$ and $\pi^- + p$ data at any given energy are very similar. The only systematic difference is in the region of the dip between the diffraction peak and the secondary peak (see Fig. 2). Here the $\pi^- + p$ cross section is systematically below the $\pi^+ + p$. This difference could be caused entirely by the greater width of the $\pi^+ + p$ diffraction peak. The falloff of the size of the secondary peak with energy occurs very systematically, as seen in Fig. 3, indicating some general dynamical origin rather than the effect of some specific resonance. Some deviation from a systematic fall-off between adjacent energy points occurs, which indicates that the dominant dynamical effect is being modified by interference from resonances. Secondary peaks at similar values of t have been seen in charge exchange,[9,10] $\Sigma^+ + K^+$ production processes, and in $K^- + p$ elastic scattering and charge-exchange scattering. The similarities of the peaks in various $\pi + p$ reactions are shown in Fig. 4, together with the η production, which does not show either a dip or a secondary maximum.[11,12] It would be interesting to have accurate data on the hypercharge exchange reactions in this region.

In the region between the secondary peak and the backward direction, the effect of resonances seems to be dominant. The cross section varies, drastically in some cases, from energy to energy, as is seen in Figs. 5 and 6. Especially striking is the peak in the 3.5-BeV/c $\pi^- + p$

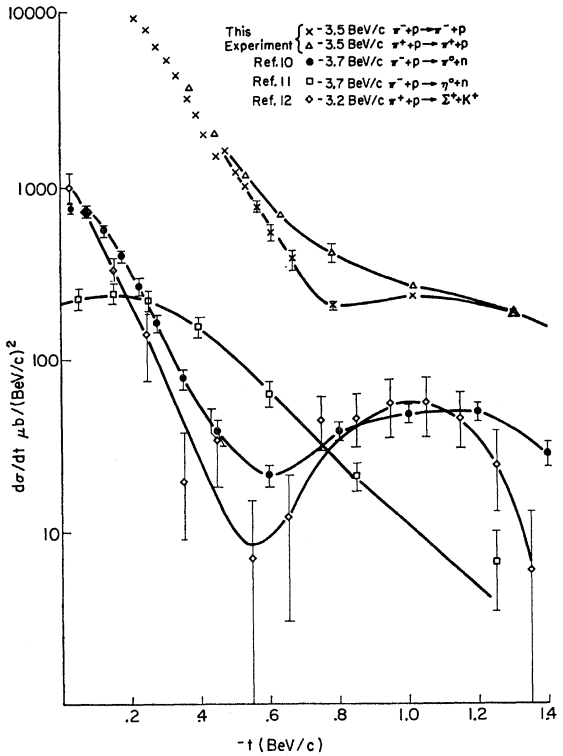

FIG. 4. Comparison of secondary-peak region for various reactions.

[6] D. Damouth, L. Jones, and M. Perl, Phys. Rev. Letters **11**, 287 (1963).
[7] D. Harting *et al.*, Nuovo Cimento **38**, 60 (1965).
[8] J. Orear *et al.*, Phys. Rev. **152**, 1162 (1966).
[9] A. Carroll *et al.*, Phys. Rev. Letters **16**, 288 (1966).
[10] P. Sondereger *et al.*, Phys. Letters **20**, 75 (1966).
[11] O. Guisan *et al.*, Phys. Letters **18**, 200 (1965).
[12] D. D. Reeder *et al.* (to be published).

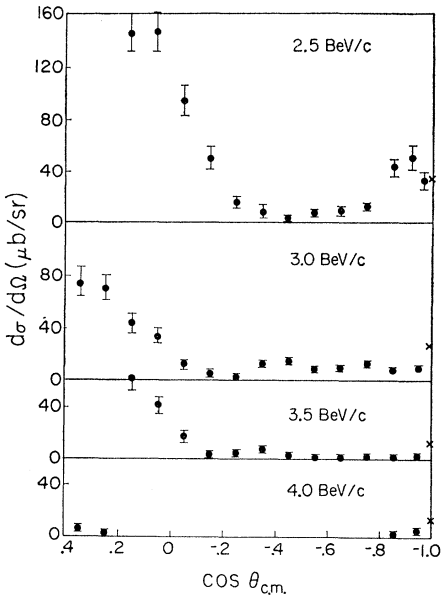

FIG. 5. π^-+p elastic scattering in the backward direction as a function of incoming momentum. 180° points from Ref. 13.

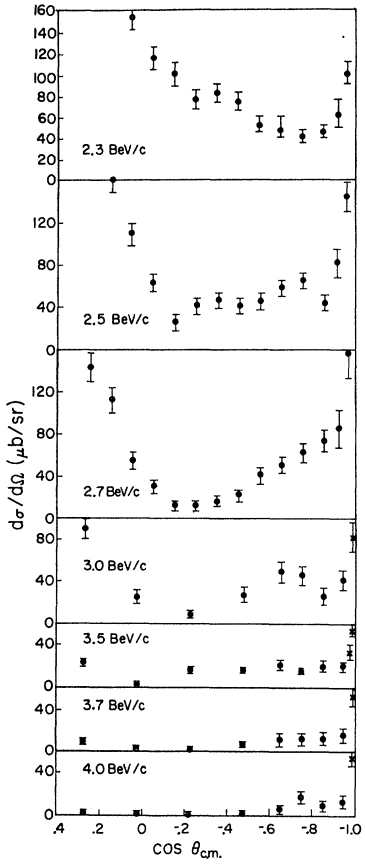

FIG. 6. $\pi^+ + p$ elastic scattering in the backward direction as a function of incoming momentum. Backward points indicated by crosses are from Ref. 14.

cross section near $\cos\theta^* = -0.3$, which is not present in either the 4.0- or 3.0-BeV/c data. This indicates a resonance near this energy. It will take very good data in this intermediate angular region at many closely spaced energies to untangle all the resonances, of which there seem to be many. The $\pi^+ + p$ cross section is systematically higher than π^- at all energies throughout the region.

In the backward direction there is a tendency for the cross section to peak as has been seen at higher energies. The backward peak in the $\pi^+ + p$ cross section is larger than that for $\pi^- + p$ by a factor of 3 or more at all energies. An extrapolation of our data to extreme backward angles is reasonably consistent with previous experiments[13–15] near 180°.

There have been several explanations of backward peaks based on baryon exchange or Regge trajectory exchange in the u channel.[16–17] It should be pointed out, however, that peaks of the order of magnitude and width observed are expected to occur as a result of the presence of resonances plus the behavior of the P_l and P_l' functions near the backward direction. Generating resonances at random, it was found that a backward peak is almost always produced.[18] Regardless of the presence or absence of other mechanisms, resonances must make sizable contributions to the backward peak at these energies.

The $\pi^+ + p$ data, in addition to the backward peak, show a tendency to be flat or show a dip and secondary peak near the backward direction at approximately the same value of u as higher-energy data.[19,20] The explanation for this behavior at higher energies in terms of Regge trajectories[21] in the u channel modified somewhat by resonance effects would naturally extend to this lower-energy region.

ACKNOWLEDGMENTS

We would like to thank the staff of the ZGS for the operation of the accelerator, L. Jones, M. Longo, and O. Overseth for help in the early stages of the experiment, and M. Ross for many useful discussions.

[13] S. Kormanyos *et al.*, Phys. Rev. Letters **16**, 709 (1966).
[14] W. Baker *et al.*, Phys. Letters **23**, 605 (1966).
[15] T. Dobrowolski *et al.* (to be published).
[16] R. Heinz and M. Ross, Phys. Rev. Letters **14**, 1091 (1965).
[17] V. Barger and D. Cline, Phys. Rev. Letters **16**, 913 (1966).
[18] Details of this to be published by N. Dikmen and M. Ross.
[19] W. R. Frisken *et al.*, Phys. Rev. Letters **15**, 313 (1965).
[20] H. Brody *et al.*, Phys. Rev. Letters **16**, 828 (1966).
[21] C. B. Chiu and J. D. Stack, Phys. Rev. **153**, 1575 (1967).